Surface capping layer prepared from the bulky Tetradodecylammonium bromide as an efficient perovskite passivation layer for high-performance perovskite solar cells

Seid Yimer Abate<sup>a</sup>, Surabhi Jha<sup>b</sup>, Guorong Ma<sup>b</sup>, Jawnaye Nash<sup>a</sup>, Nihar Pradhan<sup>a</sup>, Xiaodan Gu<sup>b</sup>,

Derek Patton<sup>b</sup>. Oilin Dai<sup>a\*</sup>

<sup>a</sup> Department of Chemistry, Physics, and Atmospheric Sciences, Jackson State University, Jackson,

MS, 39217, United States

<sup>b</sup> School of Polymer Science and Engineering, Center for Optoelectronic Materials and Devices,

The University of Southern Mississippi, Hattiesburg, MS, 39406, United States.

\* Corresponding author: Q. Dai, Email: qilin.dai@jsums.edu

**Abstract** 

The power conversion efficiency (PCE) of perovskite solar cells (PSCs) increased and levels with

silicon solar cells, however, its commercialization has not yet been realized because of its poor

long-term stability. One of the primary causes of the PSCs device instability is the large

concentration of defects in the polycrystalline perovskite film. Such defects limit the device

performance besides triggering hysteresis and device instability. In this study.

tetradodecylammonium bromide (TDDAB) was used as a post-surface modifier to suppress the

density of defects from the mixed perovskite film (CsFAMA). The XPS and FTIR analysis

validated TDDAB binds to the mixed perovskite through hydrogen bonding. The XRD and 2D-

GIWAXS study uncovered the TDDAB modification formed a capping layer of

(TDDA)<sub>2</sub>PbI<sub>1.66</sub>Br<sub>2.34</sub> on the surface of the 3D perovskite. The single charge transport device

prepared from TDDAB modified perovskite film revealed both the electron and hole defects

considerably repressed due to the modification. Consequently, the modified device displayed a

1

champion PCE of 21.33%. The TDDAB surface treatment not only enhances the PCE as well the bulky cation of the TDDAB formed a hydrophobic capping surface (water contact angle of 93.39°) and safeguards the underlayer perovskite from moisture. As a result, the modified PSC has exhibited almost no performance loss after 30 days in air (RH≈40%).

# Keywords

Surface passivation, defects, traps, grain boundary, tetradodecylammonium bromide, perovskite solar cells

#### Introduction

The PCE of PSCs has shown above 25% and levels with the commercially available silicon solar cells due to its superior absorption coefficient, favorable electron-hole dissociation energy, long charge carrier diffusion length, and efficient charge transport properties. However, unlike the silicon solar cells a PSCs prepared from a polycrystalline perovskite this film contains a high density of defects which limits the PSC to attain its theoretically predicated PCE. The defects triggered undesirable hysteresis, and diminished photoluminescence, leading to retard charge transport, which resulted in inferior solar cell performance and device instability. These defects are unavoidable because of the ionic nature of perovskite. Therefore, it is necessary to modify the perovskite film to repress defects, improve PCE, eradicate hysteresis, and enhance the stability of the PSC.

There are two approaches to suppress defects from the polycrystalline perovskite film. The first one is to replace the polycrystalline perovskite with a single perovskite crystal in which there is no grain boundaries (GBs), however, this approach is challenging because it is difficult to grow big enough perovskite single crystal for solar cell application. The second approach is to passivate the

polycrystalline perovskite film. The latter approach is inexpensive, scalable, and effective technique to suppress the density of defects from the perovskite layer. Various ammonium salt molecules had been utilized to passivate the perovskite film and demonstrated an enhancement in PCE and long-term stability of the PSC device.<sup>3-15</sup> However, most of the findings passivated only either positively or negatively charged defects, not both at the same time. Some studies have shown the successful passivation of both positively and negatively charged defects.<sup>16-26</sup> Therefore, it is an urgent task to develop a single molecule to passivate both types of defects.

In this study, we reported bulky symmetrical quaternary ammonium halide TDDAB molecule to passivate the perovskite defects. We employed a post-surface modification strategy and mild temperature annealing to investigate the sole role of TDDAB on the surface passivation of the perovskite layer without TDDAB interfering in the nucleation and crystallization stage of the perovskite layer. Because of its bulky size, the TDDA<sup>+</sup> will not incorporate in the 3D perovskite instead modify only the perovskite surface and grain boundaries. The spectroscopy studies including FTIR, XRD, 2D-GIWAXS, XPS, and SEM results clearly revealed that TDDAB could react with the CsFAMA precursor components and modify both the uncoordinated Pb<sup>2+</sup> and halide defects. Therefore, the TDDAB modified film showed superior photoluminescence (PL) and charge recombination resistance due to the suppressing of both surface and electronic defects. Subsequently, the TDDAB modified perovskite device demonstrated enhanced V<sub>oc</sub> and FF which signifies a successful suppression of defects. Intriguingly, the TDDAB interacted with the excess PbI<sub>2</sub> / PbBr<sub>2</sub> and formed a low-dimensional capping layer of (TDDA)<sub>2</sub>PbI<sub>1.66</sub>Br<sub>2.34</sub> on the surface of the 3D perovskite. The ultraviolet photoelectron spectroscopy (UPS) investigation demonstrated that the TDDAB-modified perovskite exhibited suitable energy level alignment with the spiro-OMeTAD, leading to improved device performance. Consequently, the TDDAB-treated PSCs exhibited a champion PCE of 21.33% simultaneously with a promising stability profile. The modified structure improved the stability of perovskite materials by strengthening the electrostatic interactions between the layers. Moreover, TDDAB formed a hydrophobic (93° water contact angle) capping layer as a result the modified device-maintained *ca.* 98% of its initial PCE after 720 h in the air (RH of ~40%).

# **Experimental Section**

**Materials:** FTO substrate and all chemicals used in this study are obtained from the same company with our previous report.<sup>27</sup> TDDAB purchased from Sigma-Aldrich.

**Device Fabrication:** The FTO cleaned and  $SnO_2$  prepared following literature.<sup>27</sup> Then the substrate transferred to a nitrogen glove box ( $O_2$  and  $H_2O$  are < 0.01 ppm) to spin-coat perovskite, TDDAB, and spiro-OMeTAD layers.

The mixed perovskite with a composition of Cs<sub>0.05</sub>(FA<sub>0.83</sub>MA<sub>0.17</sub>)<sub>0.95</sub>Pb(I<sub>0.83</sub>Br<sub>0.17</sub>)<sub>3</sub> is prepared by mixing FAI (1.17 mM), PbI<sub>2</sub> (1.27 M), MABr (0.23 mM), PbBr<sub>2</sub> (0.25 mM) in DMF: DMSO (4:1 v/v). 64μL CsI (1.5 mM CsI in DMSO) was added to get the final composition. The mixed perovskite was spin-coated at 1000 rpm for 10 s and 6000 rpm for 20 s followed by chlorobenzene dripping in the last 5 s. Subsequently, the film was annealed 100 °C for 1h. Next, various concentrations of TDDAB in 2-propanol were deposited on perovskite film following literature.<sup>27</sup> The optimized TDDAB concentration for the champion solar cell is 2mM. Afterwards, spiro-OMeTAD and Au (~70 nm) successively deposited following the procedure described in literature.<sup>27</sup>

**XRD film preparation:** To study the interaction of PbI<sub>2</sub> and TDDAB, PbI<sub>2</sub>:TDDAB (1:1 molar ratio) and PbI<sub>2</sub>:TDDAB (1:2 molar ratio) was mixed in DMF: DMSO (4:1 v/v) at 70 °C for 30min.

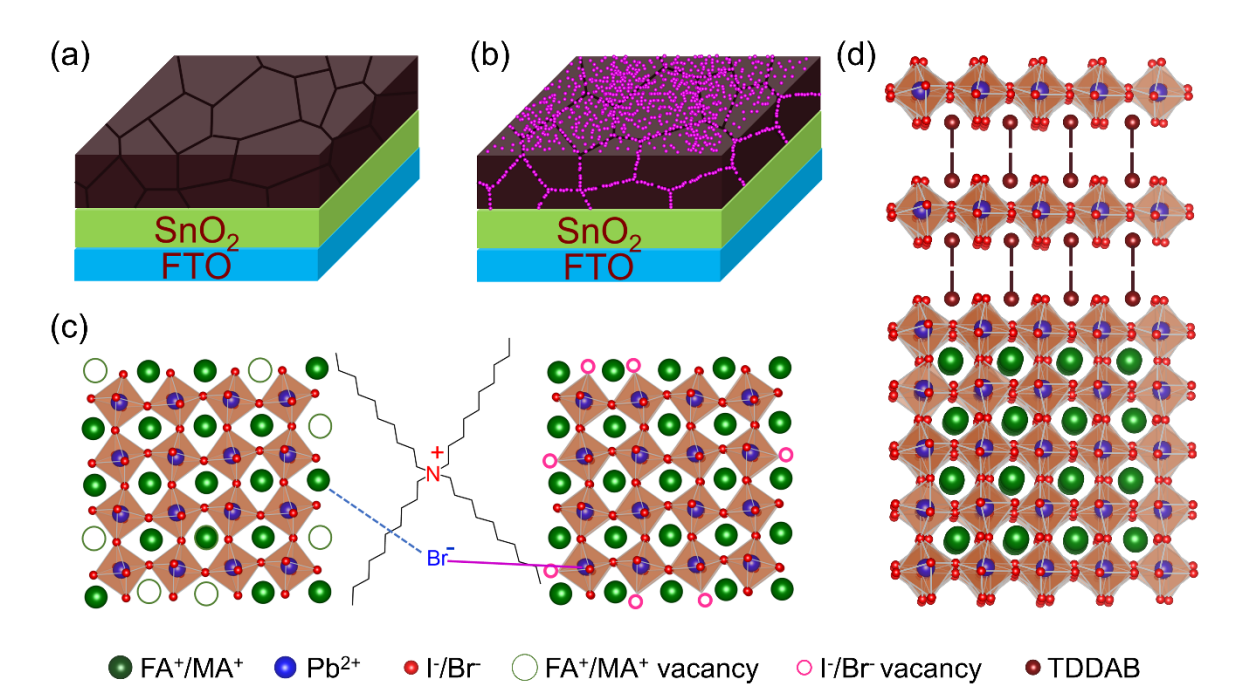
Then the solution is spin coated on glass at 1000 rpm for 10 s and 6000 rpm for 20 s followed by 70 °C backing for 5min.

**Film and device characterizations:** The perovskite and modified perovskite films were characterized by XRD, FTIR, XPS, UPS, SEM, UV-Vis, PL, and TRPL, which are the same as our previous work.<sup>27, 28</sup> Similarly, I-V and EQE of the devices characterized following the conditions provided in reference, where the aperture area of the cell is 0.1cm<sup>2</sup>.<sup>27, 28</sup>

#### **Results and Discussion**

Schematic representation of the control and passivated perovskite films are illustrated on Scheme 1a-b. TDDAB can passivate the surface and grain boundary defects of the perovskite films. The molecular interactions between TDDAB and perovskite are depicted in scheme 1c, and the low-dimensional perovskite structure formed presented in scheme 1d.<sup>29,30</sup> Both the I<sup>-</sup>/Br<sup>-</sup> vacancies and Pb<sup>2+</sup> ions were modified by the TDDAB due to the zwitterionic nature of TDDAB.

To study the interactions involved between TDDAB and CsFAMA we employed FTIR and XPS. The FTIR peaks at 3399 cm<sup>-1</sup> (asym. C-N stretch), 3266 cm<sup>-1</sup> (sym. NH<sub>3</sub><sup>+</sup> stretch), 1472 cm<sup>-1</sup> (sym. NH<sub>3</sub><sup>+</sup> bend), 958 cm<sup>-1</sup> (C-N stretch), and 905 cm<sup>-1</sup> (CH<sub>3</sub>-NH<sub>3</sub><sup>+</sup> rock) for the control perovskite are shifted to 3391 cm<sup>-1</sup>, 3261 cm<sup>-1</sup>, 1467 cm<sup>-1</sup>, 963 cm<sup>-1</sup> and 909 cm<sup>-1</sup>, respectively for TDDAB modified perovskite. The N-H and C-N peak shifts after TDDAB modification indicated that there is clear interaction between TDDAB and perovskite. The N1s peak in CsFAMA attributed to N-H bonds from the protonated amines (NH<sub>3</sub><sup>+</sup>) from the perovskite precursor (MABr and FAI), where the electronegative part of TDDAB (Br<sup>-</sup>) and NH<sub>3</sub><sup>+</sup> of the perovskite (emerged from MABr or FAI) form hydrogen bonding (N-H...Br).<sup>28, 31-33</sup>



Scheme 1: Schematic illustration of (a) the control perovskite film, (b) TDDAB modified perovskite film, (c) electronic defects on the control perovskite film and interaction between TDDAB and perovskite, and (d) (TDDA)<sub>2</sub>Pb I<sub>1,66</sub>Br<sub>2,34</sub>/CsFAMA.

Next, we recorded XRD of the control perovskite, various concentration TDDAB modified perovskite, and various concentration PbI2 and TDDAB mix to understand the detailed perovskite structure formed after the perovskite passivated with the bulky TDDAB. The XRD is presented in Figure 1e and Figure S1-2, where we clearly see that the PbI<sub>2</sub> / PbBr<sub>2</sub> reacted with TDDAB to form a new phase. To determine the new phase, we postulate the following two chemical reactions could take place between the excess PbI2, PbBr2 or PbI2/PbBr2 and TDDAB. The chemical (i-ii).<sup>34</sup> reactions described in equation Note perovskite are that our  $Cs_{0.05}(FA_{0.83}MA_{0.17})_{0.95}Pb(I_{0.83}Br_{0.17})_3$  composed of  $PbI_2:PbBr_2$  (0.83:0.17 molar ratio).

- i.  $0.83 \text{ mM PbI}_2 + 0.17 \text{ mM PbBr}_2 + 1 \text{ mM TDDAB} \rightarrow \text{TDDAPbI}_{1.66}\text{Br}_{1.34}$
- ii.  $0.83 \text{ mM PbI}_2 + 0.17 \text{ mM PbBr}_2 + 2 \text{ mM TDDAB} \rightarrow \text{(TDDA)}_2\text{PbI}_{1.66}\text{Br}_{2.34}$

To investigate the structure correctly, it is must to precisely quantify the excess PbI2, PbBr2 or PbI<sub>2</sub>:PbBr<sub>2</sub> in the CsFAMA perovskite layer. In general, the excess PbI<sub>2</sub>, PbBr<sub>2</sub> or PbI<sub>2</sub>:PbBr<sub>2</sub> are available on the top of the perovskite surface, however, it is complicated to determine the composition precisely. As a result, we measured the XRD of [1 mM PbI<sub>2</sub> + 1 mM TDDAB, and 1 mM PbI<sub>2</sub> + 2 mM TDDAB] as the PbI<sub>2</sub> concentration more to scrutinize the possible structure formed. Note, when we increased the ratio of PbI2:TDDAB to more than 1:2 molar ratio the composition didn't dissolve in DMF: DMSO (4:1 v/v). So, we focused only [1 mM PbI<sub>2</sub> + 1 mM TDDAB, and 1 mM PbI<sub>2</sub> + 2 mM TDDAB], and we measured the XRD (Figure S1). When we varied the PbI2:TDDAB ratio, the XRD peak signals varied, however, in both cases (TDDA)<sub>2</sub>PbI<sub>2</sub>Br<sub>2</sub> is formed (Figure S2). The strong XRD peaks at 5.7° and 11.4°, and weak XRD peaks at 6.7°, 10.1°, and 16.9°, and 23.7° were found when the PbI<sub>2</sub>:TDDAB (1:1 molar ratio) corresponding to the intermediate 1D TDDAPbI<sub>2</sub>Br and 2D (TDDA)<sub>2</sub>PbI<sub>2</sub>Br<sub>2</sub>, respectively. <sup>35, 36</sup> The peaks from the intermediate phase at 5.7° and 11.4° were suppressed as the ratio of PbI<sub>2</sub>:TDDAB increased to 1:2, where strong XRD peak at 6.7°, 10.1°, 13.4°, 16.9°, and 23.7° emerged which is indexed as (002), (004), (006), (008) and (001), respectively which indicated the formation of a 2D capping layer over the 3D perovskite film.<sup>37</sup> Which suggested the TDDAB could react with the excess PbI<sub>2</sub> / PbBr<sub>2</sub> present in our CsFAMA actual film. To verify our hypothesis, we took the XRD of the control and the optimized 2mM TDDAB-modified film (Figure 1e and Figure S2), however, we didn't detect the 2D perovskite XRD peaks which could be due to the limited sensitivity of the XRD instrument. Then, we increased the TDDAB amount to 20mM and measure XRD (Figure S2), where 2D (TDDA)<sub>2</sub>PbI<sub>2</sub>Br<sub>2</sub> peaks emerged together with the 3D perovskite peaks, which signified that there is an obvious low-dimensional perovskite phase formed on the perovskite layer. Considering our composition and the XRD results, we concluded

that (TDDA)<sub>2</sub>PbI<sub>1.66</sub>Br<sub>2.34</sub> formed on top of CsFAMA. Previously it was reported that quaternary ammonium salts could form a low-dimensional perovskite and our results corroborated with the previous reports.<sup>38</sup>

Once we understand the TDDAB could react with perovskite and encouraged by the XRD results to verify the formation of low dimensional perovskites when the optimized 2mM TDDAB was used to modify the perovskite layer, we have taken the 2D GIWAXS of the control and TDDAB (2mM) modified perovskite films (Figure 1f-h). The control film exhibited diffraction rings at 1.01Å, 1.44Å, 1.76Å, 2.02Å, 2.27Å, 2.85Å and 3.02Å corresponding to a 2-theta of 14.22°, 20.33°, 24.92°, 28.67°, 32.31°, 40.90°, and 43.46°, respectively. Intriguingly, the TDDAB-modified perovskite has shown an additional diffraction ring at low q-vectors of 0.25Å, 0.42Å, 0.74Å, and 0.84Å corresponding to a 2-theta of 3.51°, 5.90°, 10.41°, and 11.82°. This clearly demonstrated the formation of a mixture of 1D and 2D low-dimensional perovskite. Since TDDAB employed as a post-surface modifier its molecular distribution and the distribution of Pb<sup>2+</sup> determine which phase of the low-dimensional structure formed. However, our XRD clearly demonstrated when we increased the amount of TDDAB to 20mM, we observed the formation of 2D (TDDA)<sub>2</sub>PbBr<sub>2.34</sub>I<sub>1.66</sub>.

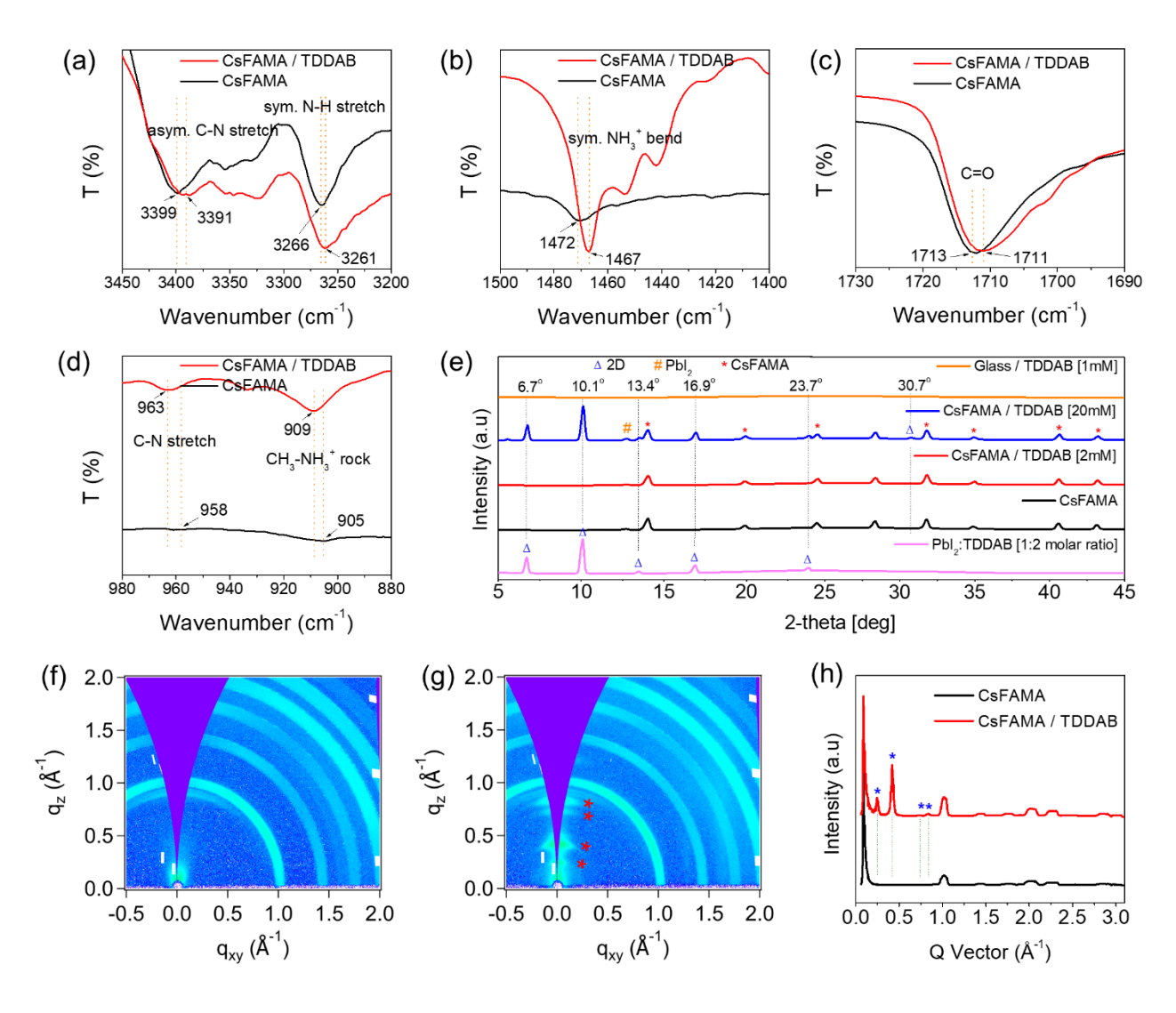


Figure 1: Characterization of the interaction between TDDAB and perovskite. (a-d) FTIR spectra of the control and TDDAB modified CsFAMA at various wavenumbers. (e) XRD of the film prepared from PbI2 reacted with TDDAB in 1:2 molar ratio, control CsFAMA film, CsFAMA modified with 2mM TDDAB film, CsFAMA modified with high concentration 20mM TDDAB film, and TDDAB film on glass (f) 2D GIWAXS scattering of CsFAMA, (g) 2D GIWAXS scattering of TDDAB-treated CsFAMA, (h) 1D GIWAXS spectra (Q Vector) comparison of the control and TDDAB modified CsFAMA. The \* represent low dimensional perovskite peak position.

To study the change in chemical composition before and after TDDAB modification, we employed X-ray photoelectron spectroscopy (XPS) and studied the high-resolution spectra of C1s, N1s, O1s, Pb4f, I3d, Br3d and Cs3d. The XPS survey spectra are presented in Figure S3. Figure 2a shows the C1s spectra, both the C-C peaks for the control and TDDAB modified film are calibrated to 284.8eV.<sup>2</sup> More importantly the C/Pb peak ratio increases drastically with the TDDAB treatment, confirming the existence of TDDAB on the surface of the perovskite. Furthermore, the peak at 287.98 eV is assigned to C=O bond for the control sample, which is shifted to 287.72 eV for the modified perovskite.<sup>2</sup> Intriguingly, the ratio of C=O/Pb decreases drastically for TDDAB-modified perovskite signifies that the capping layer formed by TDDAB modification protects the perovskite decomposition.

Figure 2b shows the N1s spectra, it is a signature peak for the presence of the ammonium group (from FAI and MABr) in the perovskite. The control perovskite exhibited only one N1s peak at 402.2 eV (assigned -NH<sub>3</sub>),<sup>2</sup> and which is shifted to 402.05 eV for the TDDAB modified film.<sup>2</sup> Besides, the modified perovskite exhibited a peak at 400.0 eV (assigned to -NH<sub>2</sub>) compared to 400.2 eV for the control films.<sup>2</sup> The N1s peak position change could demonstrated the interaction between CsFAMA and TDDAB (Br<sup>-</sup>) through hydrogen bonding to modify the halide defects. Consequently, it suppresses ion migration. Furthermore, the electronegative part of TDDAB (Br<sup>-</sup>) could interact with the uncoordinated Pb<sup>2+</sup> ions and form Pb-Br to suppress halide (I<sup>-</sup>/Br<sup>-</sup>) vacancies from the perovskite which is investigated by Pb4f XPS. The control perovskite exhibited two Pb4f XPS peaks at 142.96 eV (assigned to Pb 4f<sub>5/2</sub>) and 138.07 eV (assigned to Pb 4f<sub>7/2</sub>). These signal intensities are reduced and peaks are shifted to the lower binding energies of 142.73 eV and 137.85 eV, respectively, for the TDDAB-modified perovskite which implied the interaction between the PbI<sub>2</sub> and TDDAB.<sup>2</sup> Similarly, the I3d peak exhibited similar phenomena, where the

two peaks at 630.44 eV and 618.98 eV for the control perovskite are assigned to I3d<sub>3/2</sub> and I3d<sub>5/2</sub>, respectively. Upon TDDAB modification the I3d XPS peaks are shifted to lower binding energy of 630.15 eV and 618.76 eV, respectively, which demonstrated the local chemical environment of the [PbX<sub>6</sub>]<sup>4-</sup> modified due to the successful passivation of the uncoordinated Pb<sup>2+</sup> ions with TDDAB (Br-) which altered the binding energy. Therefore, TDDAB passivated both positively and negatively charged defects. Moreover, the Cs3d peak is presented in Figure 2e, where the control perovskite exhibited two characteristic peaks at 738.64 eV (Cs 3d<sub>3/2</sub>) and 724.62 eV (Cs 3d<sub>5/2</sub>) shifted to the lower binding energy of 738.34 eV and 724.50 eV, respectively. The O1s signal is presented in Figure 2f where the control perovskite exhibited O1s peak at 532.14eV with high ratio of O/Pb. Interestingly, the O/Pb ratio is eliminated by TDDAB modification. This suggests that the capping layer protects the perovskite decomposition significantly which boosts the cell's long-term stability. The Br3d peak is presented in Figure 2g, in which the control perovskite exhibited two characteristic peaks at 69.02eV (Br 3d<sub>3/2</sub>) and 68.13eV (Br 3d<sub>5/2</sub>) shifted to the lower binding energy of 68.86 eV and 67.91 eV, respectively. The binding energy shifts associated with the I3d, Cs3d and Br3d clearly showed the interaction of perovskite with TDDAB. Therefore, the XPS results corroborated with the XRD and 2D-GIWAXs, and all results verified that the TDDAB interacts with the perovskite and formed the capping layer.

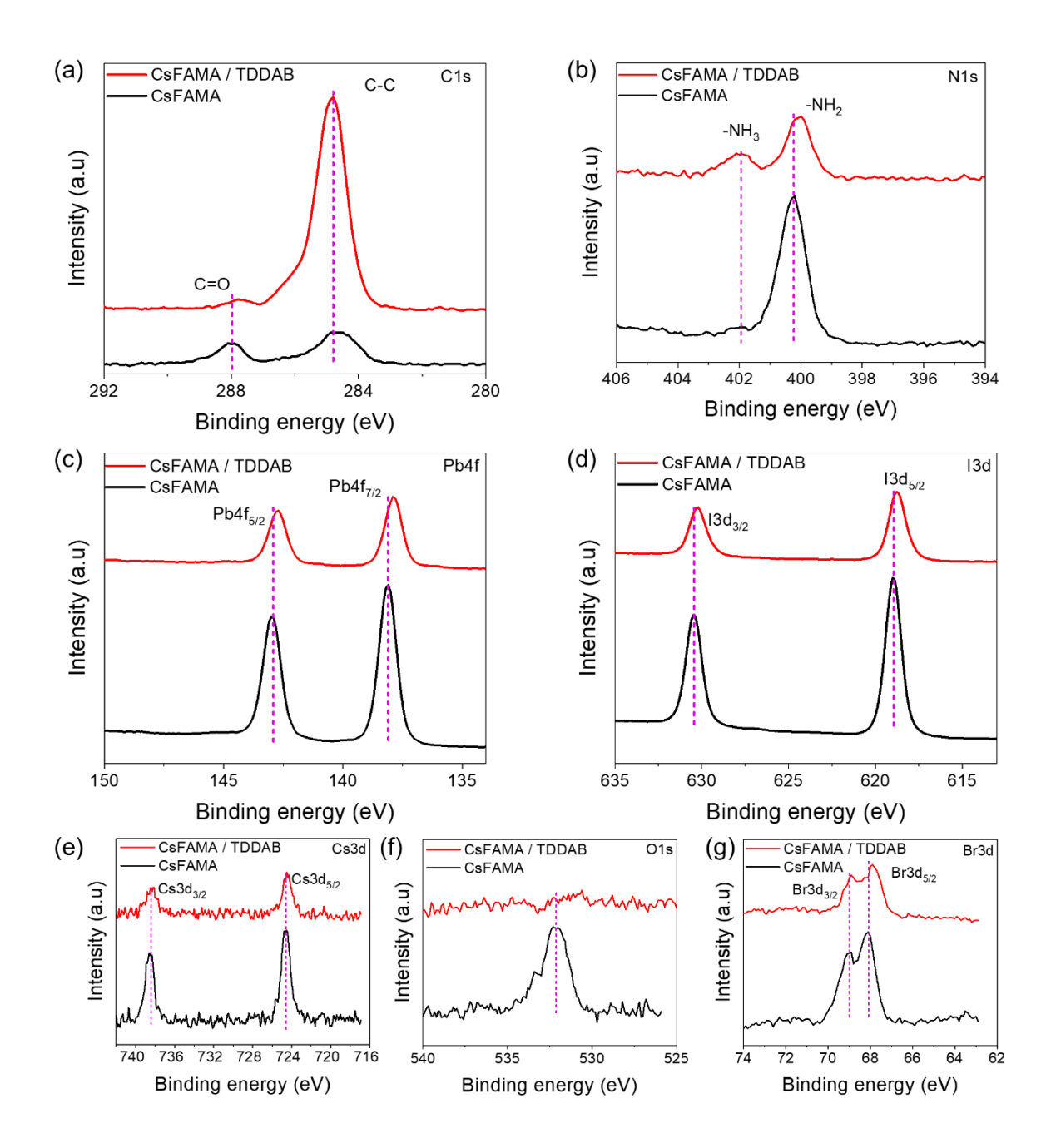


Figure 2: High-resolution XPS peaks of CsFAMA and TDDAB modified perovskite films of (a) C1s, (b) N1s, (c) Pb4f, (d) I3d, (e) Cs3d, (f) O1s, and (g) Br3d.

Next, we measured the UV-Vis absorption of the control and TDDAB-modified perovskite, in which we barely distinguish the absorption difference between the two films which implies the caping layer formed on the top surface of the perovskite are not influenced the light absorption.

The UV-vis data is presented in Figure S4.

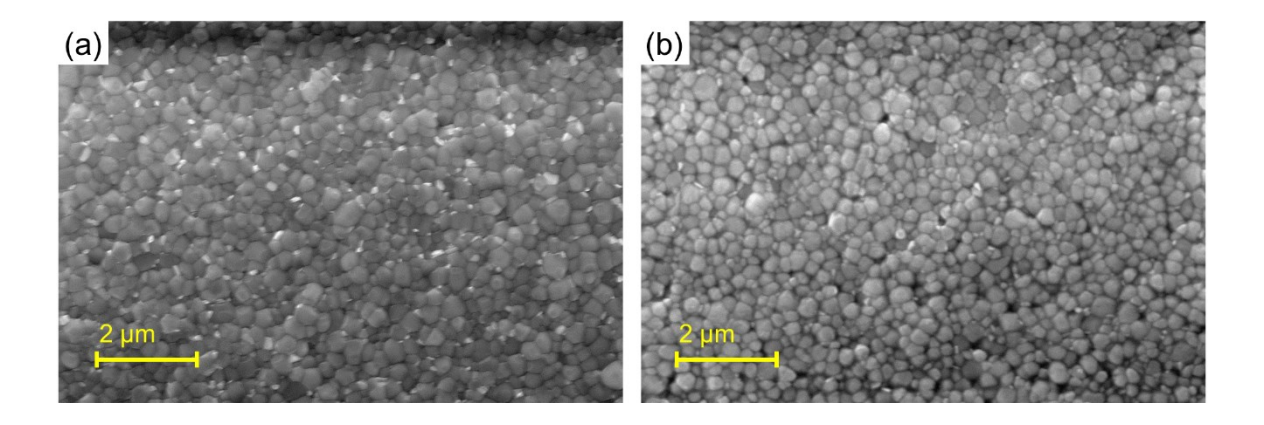


Figure 3: SEM image of (a) control perovskite, and (b) TDDAB modified perovskite.

After that, we studied the influence of TDDAB modification on the morphology of the perovskite layer. The SEM of the control perovskite and TDDAB modified perovskite are shown in Figures 3a-b. There are a lot of white spots on the control perovskites which are the excess PbI2 from the CsFAMA. After TDDAB modification these white spots are eradicated which implies that the TDDAB reacted with the excess PbI2 to form a new phase on the surface of the perovskite.<sup>39</sup> The SEM result is consistent with the XRD and GIWAXS results. Next the surface roughness of the control and TDDAB modified films are characterized by atomic force microscopy (AFM). The surface and 3-dimensional AFM for the control and modified film are presented in Figures 4a-b and Figure 4c-d respectively. The control sample exhibited a surface roughness of *ca.* 23.7nm. Upon TDDAB surface modification we have observed a flake-like structure on the surface of the perovskite surface and the surface roughness of the modified perovskite decreased to *ca.* 19.0nm. The formation of smoother film by the TDDAB could benefit interfacial contact with the hole transporting layer. Furthermore, from the AFM images, we didn't observe any significant crystal size change between the control and modified perovskite film. This signifies only a very thin layer

of capping layer is formed on the surface and GBs of the perovskite film by the post-surface modification.

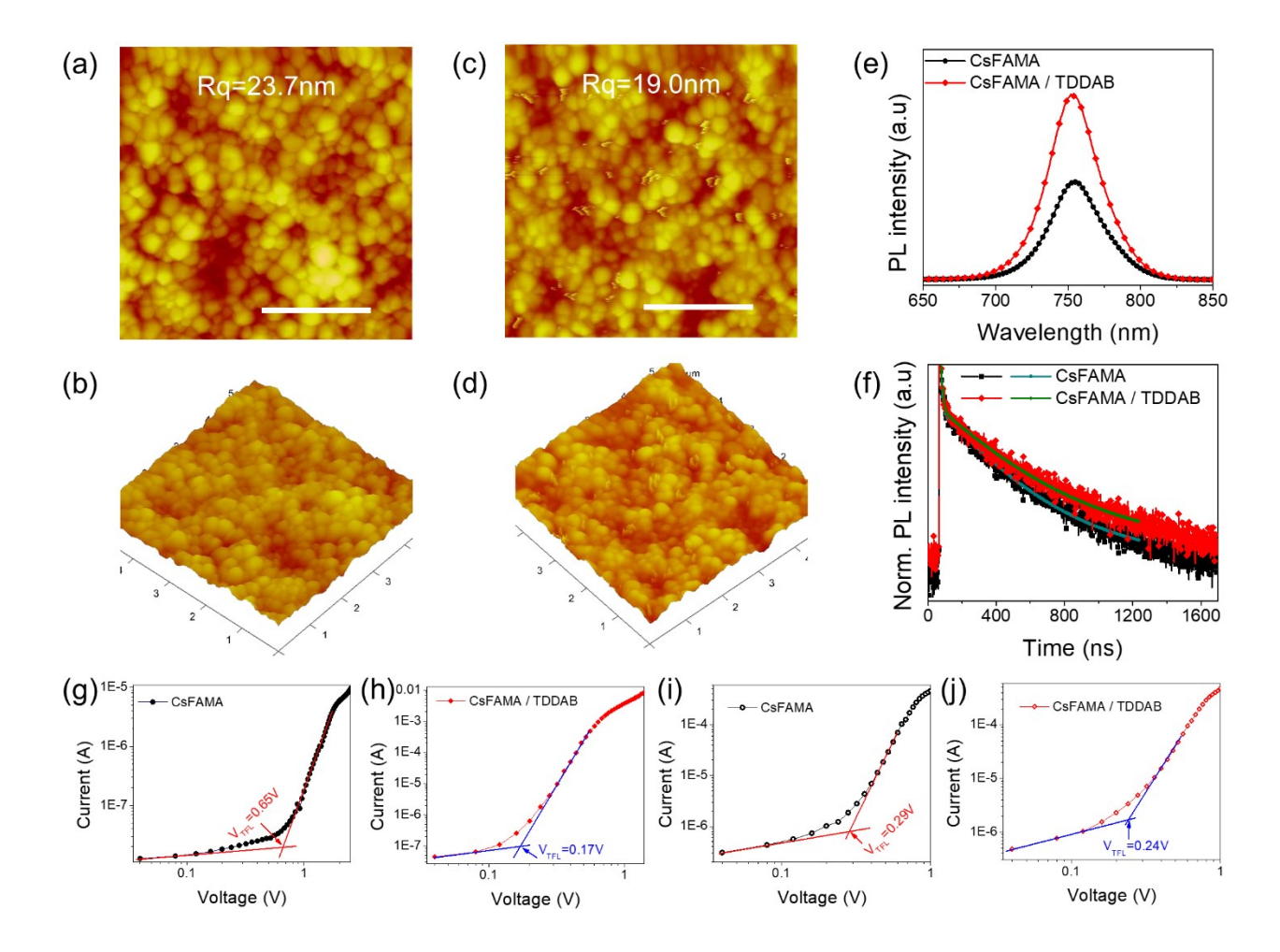


Figure 4: AFM surface and 3-dimensional image of the control (a-b) and TDDAB modified perovskite (c-d). The scale bar for the AFM surface image is 2μm. (e) Steady-state PL of the control and TDDAB modified perovskite on glass. (f) TRPL of the CsFAMA and CsFAMA / TDDAB. (g-h) Control and TDDAB modified electron-only devices, respectively. (i-j) Control and TDDAB modified hole-only device, respectively. Both electron-only and hole-only devices prepared following literature.<sup>27</sup>

Then we study the photoluminescence (PL) and time-resolved PL (TRPL) of the control and TDDAB modified film. For the PL and TRPL CsFAMA and CsFAMA / TDDAB are deposited

on glass. The light is guided from the perovskite side. The PL results are presented in Figure 4e, where the TDDAB modified film exhibited superior PL (ca. 85% PL enhancement) compared to the control sample, which signifies the TDDAB modification significantly suppressed surface and GB defects. Such defects not only influence the photoluminescence but as well PCE, hysteresis, and stability. To understand the PL in detail we have recorded TRPL spectra of the control and TDDAB modified (Figure 4f). The lifetimes of the control and TDDAB modified perovskite are fitted using a biexponential function provided in equation (1), and their average lifetime are calculated following equation (2). B<sub>1</sub> and B<sub>2</sub> represent relative amplitude, t for time,  $\tau_1$  and  $\tau_2$  are the lifetime values for the fast and slow decay, respectively.

$$Y = B_1 \exp\left(\frac{-t}{\tau_1}\right) + B_2 \exp\left(\frac{-t}{\tau_2}\right)$$
 equation (1)

$$\tau_{avg} = \frac{B_1 \tau_1^2 + B_2 \tau_2^2}{B_1 \tau_1 + B_2 \tau_2}$$
 equation (2)

The control perovskite has shown an average lifetime of 429.02 ns. With TDDAB treatment the perovskite lifetime improved considerably to 511.86 ns, which validates the suppression of defects upon TDDAB post-modification. The lifetime details are summarized in Table S1.

After that, we fabricated electron-only and hole-only devices for the control and TDDAB passivated film to quantitatively understand the density of traps the respective films. The number of traps is calculated using equation (3).

$$N_{traps} = \frac{2\varepsilon\varepsilon_0 V_{TFL}}{eL^2}$$
 equation (3)

Where  $\varepsilon$  is the relative dielectric constant of the perovskite. We adopt  $\varepsilon$ =46.9 from FAPbI<sub>3</sub><sup>40, 41</sup> because our CsFAMA consist of *ca.* 79% FAPbI<sub>3</sub>.  $\varepsilon$ <sub>0</sub> is vacuum permittivity. V<sub>TFL</sub> is trap-filled

limit voltage. e is the elementary charge. L is the thickness of perovskite and TDDAB modified perovskite and  $N_{traps}$  is the number of traps.

The electron-only devices with a structure of FTO/SnO<sub>2</sub>/CsFAMA (with and without TDDAB)/PCBM/Au are fabricated following literature procedure to quantify the number of electron traps (Figure 4g-h).<sup>27</sup> The control device exhibited 1.24×10<sup>16</sup> cm<sup>-3</sup> N<sub>traps</sub>. When the perovskite is treated with TDDAB the N<sub>traps</sub> are significantly reduced to 3.25×10<sup>15</sup> cm<sup>-3</sup> (~4-fold repression of defects). This indicates the potential for TDDAB to suppress defects. Afterwards, we analyze the number of hole traps by fabricating a hole-only device with a structure of FTO/PTAA/CsFAMA (with and without TDDAB)/Spiro-OMeTAD/Au following reference.<sup>27</sup> The hole-only device for the control and modified perovskite is presented in Figure 4i-j. The number of defects in the hole-only control device is 6.10×10<sup>15</sup> cm<sup>-3</sup>, which shrunk to 5.05×10<sup>15</sup> cm<sup>-3</sup> after TDDAB modification, which signifies the potential of TDDAB to suppress both electron and hole defects. Moreover, the passivation of perovskite by TDDAB demonstrated it passivates more to electron traps than the hole traps. For the control device, the number of electron defects is much more compared to the number of hole defects. After TDDAB modification the number of electron and hole defects decreased substantially, and relatively balanced defect numbers compared to the control device. The trap density study is consistent with the PL study. The results of N<sub>traps</sub> are summarized in Table S2.

Since the TDDAB and PbI<sub>2</sub> / PbBr<sub>2</sub> formed a new structure at the interface, we studied the influence of the new phase on the arrangement of energy level at the perovskite interface using ultraviolet photoelectron spectroscopy (UPS) and the results are presented in Figure S5a-b. The valence band maximum (VBM) of the control perovskite was calculated to be -5.6 eV. The VBM of the modified perovskite was modulated to be -5.2 eV, which is consistent with the literature

results.<sup>2</sup> The favorable energy alignment between perovskite and spiro-OMeTAD leads to efficient charge transfer. Therefore, the modified perovskite exhibited suppressed N<sub>traps</sub> and superior PL corroborated with the PL result which leads to improved PCE.

After that, we fabricated a PSC device with a structure of FTO/SnO<sub>2</sub>/CsFAMA (with and without TDDAB)/spiro-OMeTAD/Au (Figure 5a). Various concentration of TDDAB (0, 1mM, 1.5mM, 2mM, 2.5mM, 3mM) in 2-propanol were spin-coated on the perovskite film and backed at 70°C. The complete I-V optimization is summarized by a box chart in Figure S6, where the perovskite films modified with 2mM exhibited the highest optimized PCE. Figure 5b demonstrated the maximum I-V curve of the control and TDDAB modified devices. The control device exhibited a maximum PCE of 20.19% with a Jsc of 24.19mAcm<sup>-2</sup>, a Voc of 1.12V, and an FF of 74.89%. Interestingly devices modified with TDDAB demonstrated a champion PCE of 21.33% with a Jsc of 23.89mAcm<sup>-2</sup>, a Voc of 1.14V, and FF of 77.10%. The results indicated that the TDDAB modified device exhibited superior Voc and FF compared to the control devices which signifies the successful suppression of defects on the surface and GBs of perovskite film by TDDAB treatment. Furthermore, the TDDAB modified device demonstrated superior stabilized power output of 20.92% PCE when measured at maximum power point (MPP) of 0.93 V attributed to the (TDDA)<sub>2</sub>PbI<sub>1.66</sub>Br<sub>2.34</sub> top layer, while the control device exhibited a stabilized power out of 19.03% PCE when measure at MPP of 0.87 V (Figure S7). Figure 5c and Figure 5d displayed the reverse and forward bias I-V characteristic curves for the TDDAB modified and control device, respectively in which the TDDAB modified film shows less hysteresis compared to the control film. The detailed hysteresis calculations are presented in Table S3. The external quantum efficiency (EQE) of the control and TDDAB modified devices are shown in Figure 5e, where the integrated J<sub>sc</sub> of 19.39 mAcm<sup>-2</sup> and 20.23 mAcm<sup>-2</sup>, respectively. There is a discrepancy of Ca. 16%

is between the integrated J<sub>sc</sub> and the J<sub>sc</sub> measured in the I–V curve. Such inconsistency arises due to the low intensity single wavelength applied to record the EQE.<sup>1,27</sup> The discrepancy within 20% signifies a reasonable correlation.<sup>42</sup> To check the reproducibility of our fabrication process large number of TDDAB modified devices (110 samples) were fabricated and compared with the control device (34 samples). The reproducibility results are presented in Figure 5f-I, where there is a very clear improvement seen on Jsc, Voc, and FF on the TDDAB modified film. This suggests that TDDAB has a huge potential to substantially reduce the defects on the perovskite surface and GBs.

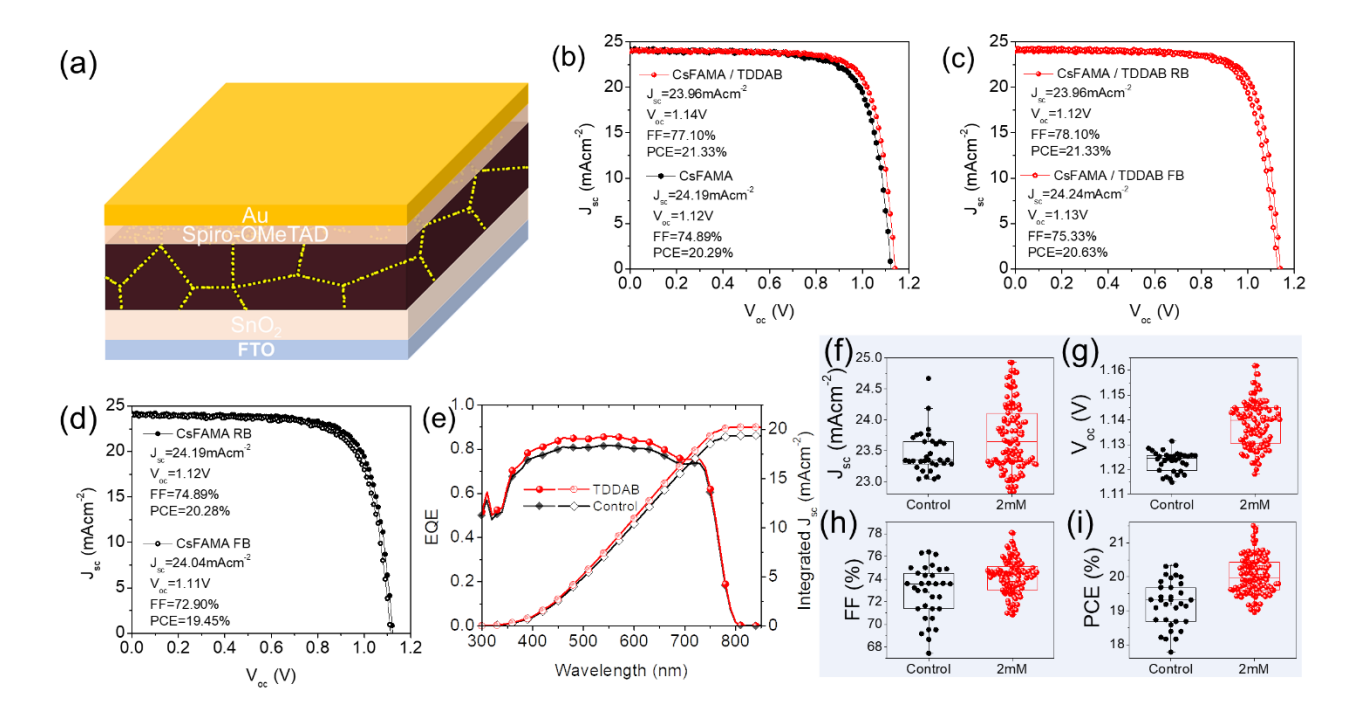


Figure 5. (a) Schematic representation of the fabricated device with a structure of FTO/SnO<sub>2</sub>/CsFAMA/TDDAB/Spiro-OMeTAD/Au. (b) J-V curve of the control and 2 mM TDDAB modified CsFAMA champion devices. (c-d) Reverse bias (RB) and forward bias (FB) J-V curve of the TDDAB modified and control device, respectively. (e) EQE and integrated J<sub>sc</sub> of the control and TDDAB modified device. Box chart comparison of the J-V parameters for the control and 2mM TDDAB modified CsFAMA device (f) J<sub>sc</sub>, (g) V<sub>oc</sub>, (h) FF and (i) PCE.

Lastly, we investigated the long-term stability of the control perovskite and TDDAB-modified perovskite layers and devices. Figure 6a-b exhibited the water contact angles of the control and TDDAB modified perovskite films, in which the control film shows a water contact angle of 53.06°. Then with TDDAB modification, the water contact angle rises to 93.39°. Large water contact angle surfaces have a huge potential to hinder the infiltration of moisture to the perovskite. To verify this, we have kept both the control and TDDAB modified devices (four samples each) in the air at (RH = 40-60%) in a dark condition for 720 hours. The TDDAB-modified devices exhibited incredible moisture tolerance than the control device. Devices fabricated with TDDAB treatment retained an average of ~99% of their initial PCE compared to an average ~82% by the control device, which signifies that TDDAB post-surface passivation improved the PCE as well the stability of the devices. The long-term stability of the control and TDDAB-modified devices are summarized in Figure 6c-f.

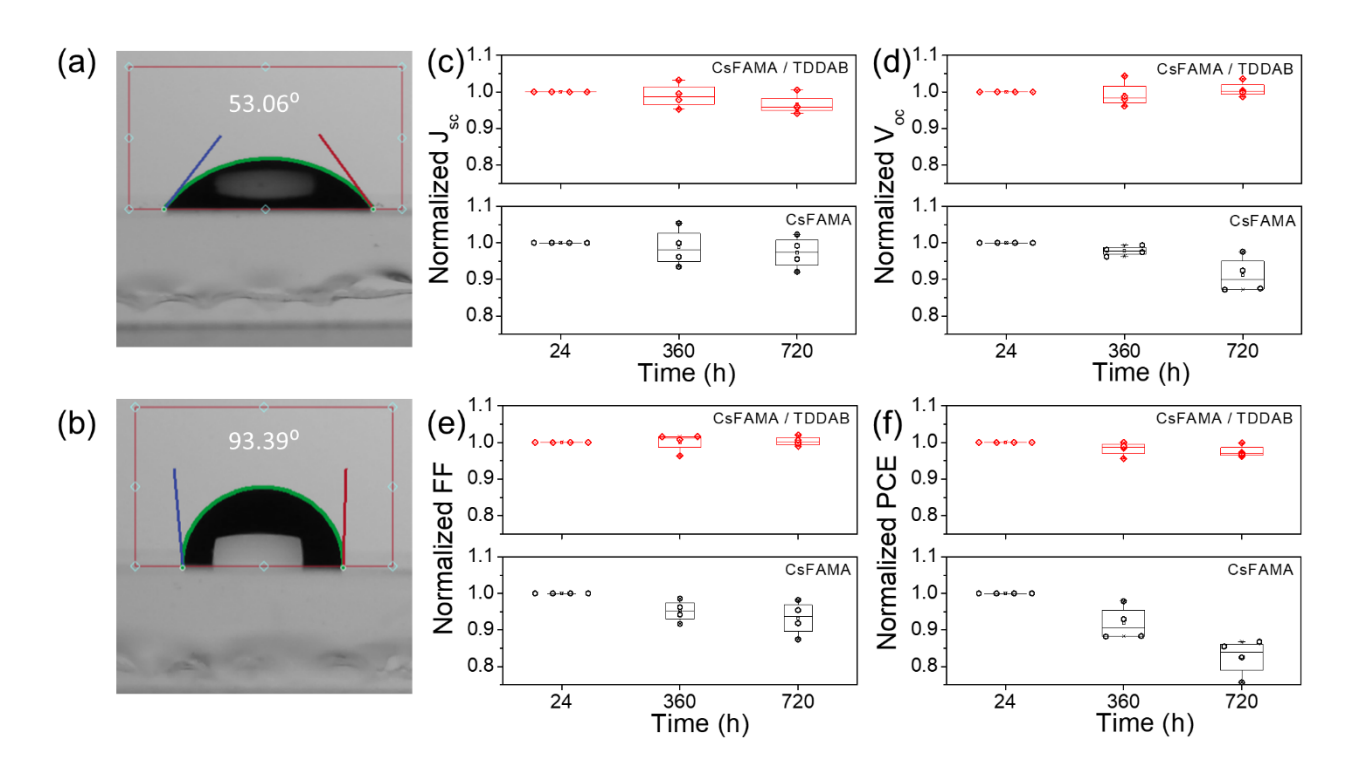


Figure 6. Water contact angle of (a) the control perovskite layer, and (b) 2mM TDDAB modified perovskite layer. Stability study of the control and 2 mM TDDAB modified solar cells, where the devices stored in air RH= 40-60% for 720 hours: (c) normalized J<sub>sc</sub>, (d) normalized V<sub>oc</sub>, (e) normalized FF, and (f) normalized PCE.

#### **Conclusions**

In summary, we have successfully developed a surface modification from TDDAB. The TDDAB reacted with the excess PbI2 and PbBr2 giving a (TDDA)2PbI1.66Br2.34 layer. The new layer the non-radiative recombination the studied suppressed for most Cs<sub>0.05</sub>(FA<sub>0.83</sub>MA<sub>0.17</sub>)<sub>0.95</sub>Pb(I<sub>0.83</sub>Br<sub>0.17</sub>)<sub>3</sub>. Moreover, both the electron and hole defect density of states are enormously reduced by the passivation. As a result, the photoluminescence and charge extraction of the passivated films increase substantially which improved both Voc and FF substantially. Consequently, the modified device delivered the maximum PCE of 21.33%. This structure also improved the stability of perovskite materials not only by strengthening the electrostatic interactions between the layers but also by forming a hydrophobic capping layer (93° water contact angle), as a result, the modified device-maintained ca. 98% of its initial PCE after 720 h in the air (RH of  $\sim$ 40%).

#### **Associated Content**

# **Supporting Information**

Additional XRD, XPS, and UV-vis spectra with a summarized table for TRPL, J-V, and SCLC provided.

# Acknowledgment

This material is based on work supported by the National Science Foundation (NSF) under Grant No. 1757220. The steady-state PL and TRPL equipment used in this work is supported by National Science Foundation Research Initiation Award: Novel Perovskite Solar Cells Based on Interface Manipulation (Award#1900047). Q. Dai thanks the support of NSF-PREM grant #DMR-1826886 for the AFM measurements by N. Pradhan.

# References

- 1. Abate, S. Y.; Wu, W.-T.; Pola, S.; Tao, Y.-T. Compact TiO2 Films with Sandwiched Ag Nanoparticles as Electron-Collecting Layer in Planar type Perovskite Solar Cells: Improvement in Efficiency and Stability. *RSC Adv.* **2018**, *8* (14), 7847-7854.
- 2. Wang, S.; Cao, F.; Wu, Y.; Zhang, X.; Zou, J.; Lan, Z.; Sun, W.; Wu, J.; Gao, P. Multifunctional 2D Perovskite Capping Layer using Cyclohexylmethylammonium Bromide for Highly Efficient and Stable Perovskite Solar Cells. *Mater. Today Phys.* **2021,** *21*, 100543.
- 3. Son, D.-Y.; Lee, J.-W.; Choi, Y. J.; Jang, I.-H.; Lee, S.; Yoo, P. J.; Shin, H.; Ahn, N.; Choi, M.; Kim, D.; Park, N.-G. Self-Formed Grain Boundary Healing Layer for Highly Efficient CH3NH3PbI3 Perovskite Solar Cells. *Nat. Energy* **2016**, *1* (7), 1-8.
- 4. Poli, I.; Eslava, S.; Cameron, P. Tetrabutylammonium Cations for Moisture-Resistant and Semitransparent Perovskite Solar Cells. *J. Mater. Chem. A* **2017**, *5* (42), 22325-22333.

- 5. Stoddard, R. J.; Rajagopal, A.; Palmer, R. L.; Braly, I. L.; Jen, A. K. Y.; Hillhouse, H. W. Enhancing Defect Tolerance and Phase Stability of High-Bandgap Perovskites via Guanidinium Alloying. *ACS Energy Lett.* **2018**, *3* (6), 1261-1268.
- 6. De Marco, N.; Zhou, H.; Chen, Q.; Sun, P.; Liu, Z.; Meng, L.; Yao, E. P.; Liu, Y.; Schiffer, A.; Yang, Y. Guanidinium: A Route to Enhanced Carrier Lifetime and Open-Circuit Voltage in Hybrid Perovskite Solar Cells. *Nano Lett.* **2016**, *16* (2), 1009-16.
- 7. Hawash, Z.; Raga, S. R.; Son, D. Y.; Ono, L. K.; Park, N. G.; Qi, Y. Interfacial Modification of Perovskite Solar Cells Using an Ultrathin MAI Layer Leads to Enhanced Energy Level Alignment, Efficiencies, and Reproducibility. *J. Phys. Chem. Lett.* **2017**, *8* (17), 3947-3953.
- 8. Kubicki, D. J.; Prochowicz, D.; Hofstetter, A.; Saski, M.; Yadav, P.; Bi, D.; Pellet, N.; Lewinski, J.; Zakeeruddin, S. M.; Gratzel, M.; Emsley, L. Formation of Stable Mixed Guanidinium-Methylammonium Phases with Exceptionally Long Carrier Lifetimes for High-Efficiency Lead Iodide-Based Perovskite Photovoltaics. *J. Am. Chem. Soc.* **2018**, *140* (9), 3345-3351.
- 9. Alharbi, E. A.; Alyamani, A. Y.; Kubicki, D. J.; Uhl, A. R.; Walder, B. J.; Alanazi, A. Q.; Luo, J.; Burgos-Caminal, A.; Albadri, A.; Albrithen, H.; Alotaibi, M. H.; Moser, J. E.; Zakeeruddin, S. M.; Giordano, F.; Emsley, L.; Gratzel, M. Atomic-Level Passivation Mechanism of Ammonium Salts Enabling Highly Efficient Perovskite Solar Cells. *Nat. Commun.* **2019**, *10* (1), 3008.
- 10. Jiang, X.; Chen, S.; Li, Y.; Zhang, L.; Shen, N.; Zhang, G.; Du, J.; Fu, N.; Xu, B. Direct Surface Passivation of Perovskite Film by 4-Fluorophenethylammonium Iodide Toward Stable and Efficient Perovskite Solar Cells. *ACS Appl. Mater. Interfaces* **2021**, *13* (2), 2558-2565.

- 11. Yang, B.; Suo, J.; Di Giacomo, F.; Olthof, S.; Bogachuk, D.; Kim, Y.; Sun, X.; Wagner, L.; Fu, F.; Zakeeruddin, S. M.; Hinsch, A.; Gratzel, M.; Di Carlo, A.; Hagfeldt, A. Interfacial Passivation Engineering of Perovskite Solar Cells with Fill Factor over 82% and Outstanding Operational Stability on n-i-p Architecture. *ACS Energy Lett.* **2021**, *6* (11), 3916-3923.
- 12. Yang, B.; Suo, J.; Mosconi, E.; Ricciarelli, D.; Tress, W.; De Angelis, F.; Kim, H.-S.; Hagfeldt, A. Outstanding Passivation Effect by a Mixed-Salt Interlayer with Internal Interactions in Perovskite Solar Cells. *ACS Energy Lett.* **2020**, *5* (10), 3159-3167.
- 13. Hauschild, D.; Seitz, L.; Gharibzadeh, S.; Steininger, R.; Jiang, N.; Yang, W.; Paetzold, U. W.; Heske, C.; Weinhardt, L. Impact of n-Butylammonium Bromide on the Chemical and Electronic Structure of Double-Cation Perovskite Thin Films. *ACS Appl. Mater. Interfaces* **2021**, (13), 53202–53210.
- 14. Du, J.; Yuan, J.; Wang, H.; Huang, F.; Tian, J. Improving the Performance and Stability of Perovskite Solar Cells through Buried Interface Passivation using Potassium Hydroxide. *ACS Appl. Energy Mater.* **2022**, *5* (2), 1914-1921.
- 15. Xi, J.; Yuan, J.; Du, J.; Yan, X.; Tian, J. A Boosting Carrier Transfer Passivation Layer for Achieving Efficient Perovskite Solar Cells. *J. Mater. Chem. C* **2022**, *10*, 9794-9801.
- 16. Zheng, X.; Chen, B.; Dai, J.; Fang, Y.; Bai, Y.; Lin, Y.; Wei, H.; Zeng, Xiao C.; Huang, J. Defect Passivation in Hybrid Perovskite Solar Cells using Quaternary Ammonium Halide Anions and Cations. *Nat. Energy* **2017**, *2* (7), 1-9.
- 17. Ye, S.; Rao, H.; Zhao, Z.; Zhang, L.; Bao, H.; Sun, W.; Li, Y.; Gu, F.; Wang, J.; Liu, Z.; Bian, Z.; Huang, C. A Breakthrough Efficiency of 19.9% Obtained in Inverted Perovskite Solar Cells by using an Efficient Trap State Passivator Cu(thiourea) I. *J. Am. Chem. Soc.* **2017**, *139* (22), 7504-7512.

- 18. Li, X.; Dar, M. I.; Yi, C.; Luo, J.; Tschumi, M.; Zakeeruddin, S. M.; Nazeeruddin, M. K.; Han, H.; Gratzel, M. Improved Performance and Stability of Perovskite Solar Cells by Crystal Crosslinking with Alkylphosphonic Acid Omega-Ammonium Chlorides. *Nat. Chem.* **2015**, *7* (9), 703-11.
- 19. Kyoungwon, C.; Junwoo, L.; Hong Il, K.; Cheol Woong, P.; Guan-Woo, K.; Hyuntae, C.; Sungjin, P.; Sang Ah, P.; Taiho, P. Thermally Stable, Planar Hybrid Perovskite Solar Cells with High Efficiency. *Energy Environ. Sci.* **2018**, (11), 3238-3247.
- 20. Yang, S.; Dai, J.; Yu, Z.; Shao, Y.; Zhou, Y.; Xiao, X.; Zeng, X. C.; Huang, J. Tailoring Passivation Molecular Structures for Extremely Small Open-Circuit Voltage Loss in Perovskite Solar Cells. *J. Am. Chem. Soc.* **2019**, *141* (14), 5781-5787.
- 21. Zhou, X.; Hu, M.; Liu, C.; Zhang, L.; Zhong, X.; Li, X.; Tian, Y.; Cheng, C.; Xu, B. Synergistic Effects of Multiple Functional Ionic Liquid-Treated PEDOT:PSS and Less-Ion-Defects S-Acetylthiocholine Chloride-Passivated Perovskite Surface Enabling Stable and Hysteresis-Free Inverted Perovskite Solar Cells with Conversion Efficiency Over 20%. *Nano Energy* **2019**, *63*, 103866.
- 22. Xiong, J.; Dai, Z.; Zhan, S.; Zhang, X.; Xue, X.; Liu, W.; Zhang, Z.; Huang, Y.; Dai, Q.; Zhang, J. Multifunctional Passivation Strategy Based on Tetraoctylammonium Bromide for Efficient Inverted Perovskite Solar Cells. *Nano Energy* **2021**, *84*, 105882.
- 23. Zheng, X.; Deng, Y.; Chen, B.; Wei, H.; Xiao, X.; Fang, Y.; Lin, Y.; Yu, Z.; Liu, Y.; Wang, Q.; Huang, J. Dual Functions of Crystallization Control and Defect Passivation Enabled by Sulfonic Zwitterions for Stable and Efficient Perovskite Solar Cells. *Adv. Mater.* **2018**, *30* (52), 1803428.

- 24. Wu, W.-Q.; Yang, Z.; Rudd, P. N.; Shao, Y.; Dai, X.; Wei, H.; Zhao, J.; Fang, Y.; Wang, Q.; Liu, Y.; Deng, Y.; Xiao, X.; Feng, Y.; Huang, J. Bilateral Alkylamine for Suppressing Charge Recombination and Improving Stability in Blade-Coated Perovskite Solar Cells. *Sci. Adv.* **2019**, *5* (3), eaav8925
- 25. Wu, W. Q.; Rudd, P. N.; Wang, Q.; Yang, Z.; Huang, J. Blading Phase-Pure Formamidinium-Alloyed Perovskites for High-Efficiency Solar Cells with Low Photovoltage Deficit and Improved Stability. *Adv. Mater.* **2020,** *32* (28), e2000995.
- 26. Zheng, D.; Peng, R.; Wang, G.; Logsdon, J. L.; Wang, B.; Hu, X.; Chen, Y.; Dravid, V. P.; Wasielewski, M. R.; Yu, J.; Huang, W.; Ge, Z.; Marks, T. J.; Facchetti, A. Simultaneous Bottom-Up Interfacial and Bulk Defect Passivation in Highly Efficient Planar Perovskite Solar Cells using Nonconjugated Small-Molecule Electrolytes. *Adv. Mater.* **2019**, *31* (40), e1903239.
- 27. Abate, S. Y.; Zhang, Q.; Qi, Y.; Nash, J.; Gollinger, K.; Zhu, X.; Han, F.; Pradhan, N.; Dai, Q. Universal Surface Passivation of Organic-Inorganic Halide Perovskite Films by Tetraoctylammonium Chloride for High-Performance and Stable Perovskite Solar Cells. . *ACS Appl. Mater. Interfaces* **2022**, *14* (24), 28044-28059.
- 28. Qi, Y.; Green, K. A.; Ma, G.; Jha, S.; Gollinger, K.; Wang, C.; Gu, X.; Patton, D.; Morgan, S. E.; Dai, Q. Passivation of Iodine Vacancies of Perovskite Films by Reducing Iodine to Triiodide Anions for High-Performance Photovoltaics. *Chem. Eng. J.* **2022**, (438), 135647.
- 29. Shpatz Dayan, A.; Wierzbowska, M.; Etgar, L. Ruddlesden–Popper 2D Chiral Perovskite-Based Solar Cells. *Small Struct.* **2022**, *3* (8), 2200051.
- 30. Ortiz-Cervantes, C.; Carmona-Monroy, P.; Solis-Ibarra, D. Two-Dimensional Halide Perovskites in Solar Cells: 2D or not 2D? *ChemSusChem* **2019**, *12* (8), 1560-1575.

- 31. Ai, Y.; Zhang, Y.; Song, J.; Kong, T.; Li, Y.; Xie, H.; Bi, D. In Situ Perovskitoid Engineering at SnO2 Interface Toward Highly Efficient and Stable Formamidinium Lead Triiodide Perovskite Solar Cells. *J. Phys. Chem. Lett.* **2021**, *12* (43), 10567-10573.
- 32. Glaser, T.; Muller, C.; Sendner, M.; Krekeler, C.; Semonin, O. E.; Hull, T. D.; Yaffe, O.; Owen, J. S.; Kowalsky, W.; Pucci, A.; Lovrincic, R. Infrared Spectroscopic Study of Vibrational Modes in Methylammonium Lead Halide Perovskites. *J. Phys. Chem. Lett.* **2015**, *6* (15), 2913-8.
- 33. Wang, R.; Xue, J.; Wang, K.-L.; Wang, Z.-K.; Luo, Y.; Fenning, D.; Xu, G.; Nuryyeva, S.; Huang, T.; Zhao, Y.; Yang, J. L.; Zhu, J.; Wang, M.; Tan, S.; Yavuz, I.; Houk, K. N.; Yang, Y. Constructive Molecular Configurations for Surface-Defect Passivation of Perovskite Photovoltaics. *Science* **2019**, *366*, 1509–1513
- 34. Ishii, A.; Miyasaka, T. Direct Detection of Circular Polarized Light in Helical 1D Perovskite-based Photodiode. *Sci. Adv.* **2020,** *6* (46), eabd3274.
- 35. Ge, C.; Zhai, W.; Tian, C.; Zhao, S.; Guo, T.; Sun, S.; Chen, W.; Ran, G. Centimeter-Scale 2D Perovskite (PEA)2PbBr4 Single Crystal Plates Grown by a Seeded Solution Method for Photodetectors. *RSC Adv.* **2019**, *9* (29), 16779-16783.
- 36. Dou, L.; Wong, A. B.; Yu, Y.; Lai, M.; Kornienko, N.; Eaton, S. W.; Fu, A.; Bischak, C. G.; Ma, J.; Ding, T.; Ginsberg, N. S.; Wang, L. W.; Alivisatos, A. P.; Yang, P. Atomically Thin Two-Dimensional Organic-Inorganic Hybrid Perovskites. *Science* **2015**, *349* (6255), 1518-21.
- 37. Hu, Y.; Spies, L. M.; Alonso-Álvarez, D.; Mocherla, P.; Jones, H.; Hanisch, J.; Bein, T.; Barnes, P. R. F.; Docampo, P. Identifying and Controlling Phase Purity in 2D Hybrid Perovskite Thin Films. *J. Mater. Chem. A* **2018**, *6* (44), 22215-22225.

- 38. Krishna, A.; Gottis, S.; Nazeeruddin, M. K.; Sauvage, F. Mixed Dimensional 2D/3D Hybrid Perovskite Absorbers: The Future of Perovskite Solar Cells? *Adv. Funct. Mater.* **2019**, *29* (8), 1806482.
- 39. Ma, C.; Leng, C.; Ji, Y.; Wei, X.; Sun, K.; Tang, L.; Yang, J.; Luo, W.; Li, C.; Deng, Y.; Feng, S.; Shen, J.; Lu, S.; Du, C.; Shi, H. 2D/3D Perovskite Hybrids as Moisture-Tolerant and Efficient Light Absorbers for Solar Cells. *Nanoscale* **2016**, *8* (43), 18309-18314.
- 40. Huang, Y.; Li, L.; Liu, Z.; Jiao, H.; He, Y.; Wang, X.; Zhu, R.; Wang, D.; Sun, J.; Chen, Q.; Zhou, H. The Intrinsic Properties of FA(1-x)MAxPbI3 Perovskite Single Crystals. *J. Mater. Chem. A* **2017**, *5* (18), 8537-8544.
- 41. Poorkazem, K.; Kelly, Timothy L. Improving the Stability and Decreasing the Trap State Density of Mixed-Cation Perovskite Solar Cells through Compositional Engineering. *Sustain*. *Energy Fuels* **2018**, *2* (6), 1332-1341.
- 42. Christians, J. A.; Manser, J. S.; Kamat, P. V. Best Practices in Perovskite Solar Cell Efficiency Measurements. Avoiding the Error of Making Bad Cells Look Good. *J. Phys. Chem. Lett.* **2015**, *6* (5), 852-7.

# TOC

